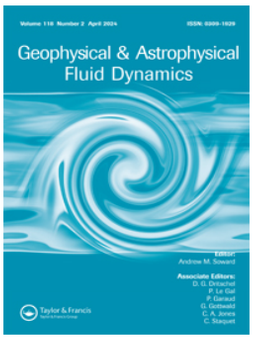

Geophysical & Astrophysical Fluid Dynamics

ISSN: 0309-1929 (Print) 1029-0419 (Online) Journal homepage: www.tandfonline.com/journals/ggaf20

Thermochemical convection in a slowly rotating spherical shell: a transition between prograde and retrograde flows

J. Šimkanin, P. Guba, J. Kyselica & M. Y. Nnaedu

To cite this article: J. Šimkanin, P. Guba, J. Kyselica & M. Y. Nnaedu (2024) Thermochemical convection in a slowly rotating spherical shell: a transition between prograde and retrograde flows, Geophysical & Astrophysical Fluid Dynamics, 118:2, 120-129, DOI: 10.1080/03091929.2024.2345611

To link to this article: https://doi.org/10.1080/03091929.2024.2345611

GEOPHYSICAL & ASTROPHYSICAL FLUID DYNAMICS
2024, VOL. 118, NO. 2, 120–129
https://doi.org/10.1080/03091929.2024.2345611

Taylor & Francis
Taylor & Francis Group

Thermochemical convection in a slowly rotating spherical shell: a transition between prograde and retrograde flows

J. Šimkanin[a], P. Guba[b], J. Kyselica[a] and M. Y. Nnaedu [b]

[a]Institute of Geophysics, Czech Academy of Sciences, Prague 4, Czech Republic; [b]Faculty of Mathematics, Physics and Informatics, Comenius University, Bratislava, Slovakia

ABSTRACT

We numerically investigate thermochemically-driven convection in a spherical shell at a high Ekman number for a range of Rayleigh numbers, Prandtl numbers and buoyancy ratios. Rotating convection displays a nearly axisymmetric large-scale structure and appears mostly unaffected by the nature (thermal or chemical) of the driving buoyancy source. We observe both precession directions, prograde and retrograde, of convection structures and identify a snap-through transition between the prograde and retrograde flows in the parameter space spanned by the Rayleigh and Prandtl numbers. Equatorially wall-attached and spiralling columnar convection structures, which typically emerge in rapidly rotating shells, are not observed.

ARTICLE HISTORY
Received 23 February 2023
Accepted 17 April 2024

KEYWORDS
Spherical shells; thermochemical convection; codensity formulation; prograde flows; retrograde flows

1. Introduction

The radiogenic heating and solidification processes that take place at the inner – outer core boundary of the Earth are the energy source for the outer-core convection and the hydromagnetic dynamo. These processes are the source of two types of bouyancy – thermal and compositional. Numerical models of convection in rotating spherical shells are mainly concerned with thermal sources (Braginsky and Roberts 1995, Glatzmaier and Roberts 1997, Christensen and Wicht 2008, Jones 2011; Šimkanin and Hejda 2013), although in recent years there has also been an emphasis on models that take into account the compositional sources. In general, those two sources are independent, but due to the turbulent nature of convection in the Earth's core, the thermal and compositional fields can be combined into a single "codensity" field. The codensity concept provides a simplified description of convective processes in planetary cores involving a single effective source distribution and a single effective value of codensity diffusivity (Braginsky and Roberts 1995, Lister and Buffett 1995, Aubert *et al.* 2008, Christensen and Wicht 2008).

The onset of thermal convection in slowly rotating fluid shells was first studied by Geiger and Busse (1981). They found that the preferred convection mode was axisymmetric with the spherical harmonic degree $l = 1$, provided the fluid shell was sufficiently thick. The onset of thermal convection at different Prandtl numbers was then studied by Zhang and Busse (1987). Their analysis was extended to the nonlinear regime by Ardes *et al.* (1997).

CONTACT J. Šimkanin jano@ig.cas.cz

Both analyses conclude that at high Ekman numbers (the slow-rotation regime) the excited modes drift in the retrograde direction, while at low Ekman numbers (the fast-rotation regime) they propagate in the prograde direction. At moderate and high Prandtl numbers, a columnar convection is excited, while at low Prandtl numbers, three different modes appear: retrograde inertial modes, prograde wall-attached modes and prograde spiralling columnar modes (see figure 17 in Zhang and Busse 1987).

Šimkanin *et al.* (2018) investigated the thermochemical convection and hydromagnetic dynamos in a rotating spherical shell using the codensity formulation with various buoyancy sources (the secular cooling from the mantle, the buoyancy sources due to freezing at the inner core boundary, and the combination of the two sources). In the non-magnetic cases, they found that for Prandtl numbers smaller than the Ekman numbers, the convection takes the form of inertial oscillations with retrograde propagation. Otherwise, large-scale spiralling columnar convection drifting in the prograde azimuthal direction was observed. These results are consistent with findings of Zhang and Busse (1987), Ardes *et al.* (1997) and also Kimura *et al.* (2011) and Horn and Schmid (2017).

The complex behaviour of convection described above provides a motivation to investigate a nonlinear development of slow-rotating thermochemical convection at different Prandtl numbers. This regime broadly corresponds to the low-Taylor number regime in the linear stability analysis of Zhang and Busse (1987) (see their figure 17, the region to the left of line I). The model is described and governing equations are given in section 2. Our findings are presented in section 3. Finally, discussion and conclusions are provided in section 4.

2. Model and basic equations

We use a model of Aubert *et al.* (2009) to simulate thermochemical convection in a rotating spherical shell. Under the Boussinesq approximation, the velocity, $\boldsymbol{u}$, the codensity, C and the pressure, p, are governed by

$$E\left[\frac{\partial \boldsymbol{u}}{\partial t} + (\boldsymbol{u}\cdot\boldsymbol{\nabla})\,\boldsymbol{u} - \nabla^2\boldsymbol{u}\right] + 2\mathbf{1}_z \times \boldsymbol{u} = -\boldsymbol{\nabla}p + Ra\,C\frac{\boldsymbol{r}}{r_o}, \tag{1a}$$

$$\frac{\partial C}{\partial t} + (\boldsymbol{u}\cdot\boldsymbol{\nabla})\,C = \frac{1}{Pr}\nabla^2 C + S_C, \tag{1b}$$

$$\boldsymbol{\nabla}\cdot\boldsymbol{u} = 0. \tag{1c}$$

The conventional spherical coordinate system with the radial coordinate r, the azimuthal angle θ, and the polar angle ϕ is used. The incompressible fluid occupies the spherical shell $r_i < r < r_o$, where r_i and r_o are the inner and outer core radii. The shell rotates with the angular velocity Ω about an axis described by the unit vector $\mathbf{1}_z$. We employ the shell gap $L = r_o - r_i$ as a length scale and the viscous time L^2/ν as a time scale. The aspect ratio of the spherical shell, r_i/r_o, is set to 0.35. The velocity, the codensity and the pressure are non-dimensionalized with the velocity scale ν/L, the codensity scale $F/(4\pi\nu L)$ and the pressure scale $\rho\nu^2/L^2$. Here, ν is the kinematic viscosity and F is a total codensity flux. The dimensionless parameters appearing in (1) are the Prandtl number, the Ekman number,

and the Rayleigh number, defined respectively as

$$Pr = \frac{\nu}{\kappa}, \quad E = \frac{\nu}{\Omega L^2} \quad \text{and} \quad Ra = \frac{Fg_0}{4\pi\rho\nu^2\Omega}, \tag{2}$$

where κ is the thermal diffusivity and g_o is the gravitational acceleration at $r = r_o$.

A detailed description of the thermochemical model is provided by Aubert *et al.* (2009) and also Šimkanin *et al.* (2018), so here we only briefly describe its basic features. The model is based on the codensity formulation, in which the temperature and concentration fields are combined into a single scalar codensity field related to the mass anomaly (buoyancy density). The formulation assumes identical diffusivities of heat and chemicals.

The codensity equation (1b) involves a source term S_C, which we take as

$$S_C = 3\frac{1 - 2f_i}{r_o^3 - r_i^3}. \tag{3}$$

Here f_i is the buoyancy ratio at the inner boundary, $f_i = F_i/F$, where the total codensity flux $F = F_i + F_o$, and F_i and F_o are the codensity fluxes at the inner and outer boundaries. The release of latent heat and light elements at the inner boundary creates the positive F_i, while F_o can take either sign. However, the total flux F must be positive for convection to occur (Aubert *et al.* 2009, Šimkanin *et al.* 2018).

Following Davies and Gubbins (2011), the source term S_C given in (3) can be interpreted in terms of two components. The first component comes from the reference state and has the thermal and compositional parts. The thermal part contains the buoyancy sinks due to the adiabatic gradient and the secular change (cooling at the outer boundary, the latent-heat release and the radiogenic heating). The compositional part is associated with the release of light components during freezing of the core. The second component captures the remaining codensity sources, defined so as the rate of change of the average departure from the reference state vanishes. For further details, see Braginsky and Roberts (1995) and Kutzner and Christensen (2002).

We assume the non-penetrating boundary conditions for the velocity field at both boundaries, the no-slip condition at the outer boundary and the stress-free condition at the inner boundary. We initialise the velocity to a Gaussian noise and the codensity to a conductive profile

$$C_0(r) = C_i + Pr\left(f_i - \frac{1}{3}S_C\right)\left(\frac{1}{r} - \frac{1}{r_i}\right) - \frac{1}{6}PrS_C\left(r^2 - r_i^2\right), \tag{4}$$

which is a steady-state spherically-symmetric solution to the codensity equation (1b).

3. Numerical results

Equations (1) are integrated numerically using the geodynamo simulation code called PARODY (Dormy 1997, Dormy *et al.* 1998, Aubert *et al.* 2008, Raynaud and Dormy 2013), a semi-spectral code that implements the spherical harmonics decomposition in the lateral directions, a second-order finite-difference scheme in the radial direction and the time integration via the implicit second-order Crank–Nicolson scheme. The spatial resolution

is set to $(N_r \times N_\theta \times N_\phi) = (185 \times 96 \times 192)$, where N_r, N_θ and N_ϕ are the numbers of grid points in the respective directions.

For our series of simulations, we set the Ekman number to $E = 10^{-1}$, a factor of 10^2 higher than the value relevant to the extreme conditions of Earth's core (Christensen *et al.* 2001). We carried out simulations for increasing Prandtl numbers Pr between 10^{-5} and 10^{-1}, giving rise to a slowly rotating thermochemical convection regime. This broadly matches the small-Taylor-number regime in the linear stability of Zhang and Busse (1987). The minimum critical Rayleigh number, Ra_c, for the onset of thermal convection depends on E and Pr (e.g. Zhang 1992). The simulations are conducted for the increasing forcing of Ra/Ra_c between 5 and 1.2×10^4. We fix f_i to 0.5, which corresponds to secular cooling at the core/mantle boundary. The simulation is run to $t = 5$ in all cases.

We present the sample results found for $Ra/Ra_c = 5 \times 10^3$. Figure 1 shows meridional cross-sections, taken at $\phi = 0$, of codensity and flow-field components for $Pr = 10^{-3}$ (top panel) and $Pr = 10^{-2}$ (bottom panel). Figure 2 shows the corresponding results in the equatorial cross-sections. The snapshots are taken at $t = 5$. We see that increasing the Prandtl number changes the azimuthal flow from purely retrograde ($u_\phi < 0$) to purely prograde ($u_\phi > 0$). The latitudinal structure of poloidal and toroidal fields is unchanged, but

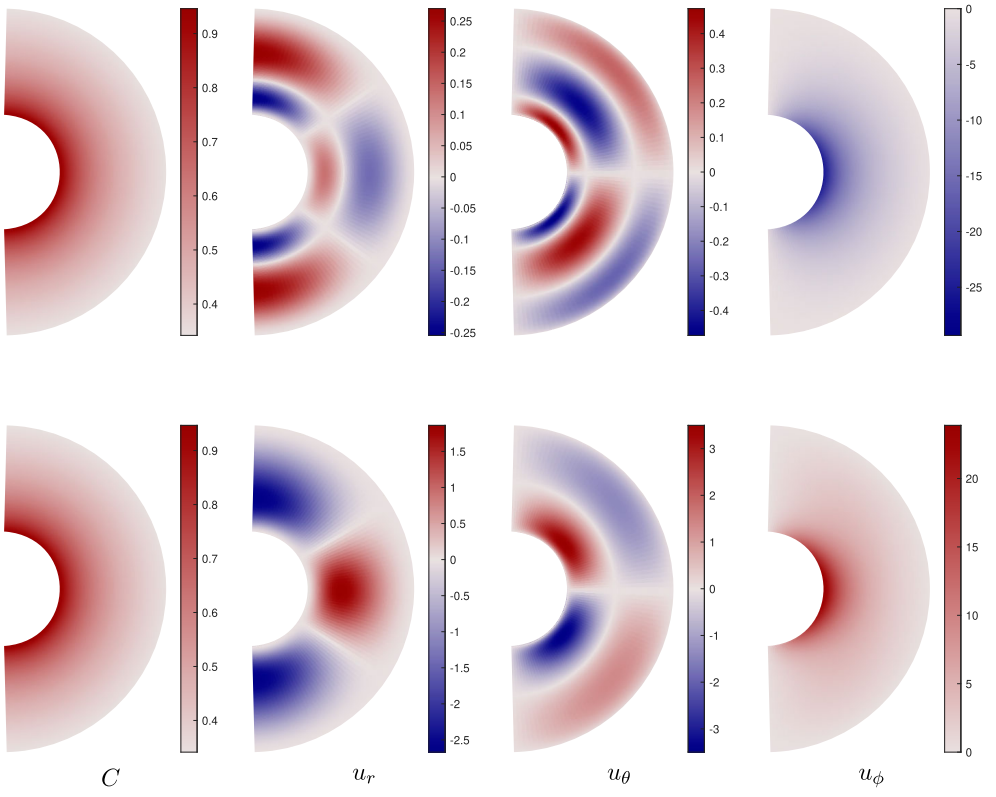

Figure 1. Meridional cross-sections of the codensity C and the velocity components u_r, u_θ and u_ϕ. Note that for $Pr = 10^{-3}$ (top panel), the azimuthal flow u_ϕ has a prograde direction, while for $Pr = 10^{-2}$ (bottom panel), the azimuthal flow u_ϕ has a retrograde direction. The snapshots were taken at $t = 5$. The other parameter values are $Ra/Ra_c = 5 \times 10^3$ and $f_i = 0.5$.

the radial structure of the poloidal flow changes from three radially-stacked cells in the retrograde regime to two cells in the prograde regime. The azimuthal flow u_ϕ is localised near the equator and the inner-sphere boundary in both regimes. In terms of magnitude, the u_ϕ component dominates the u_r and u_θ components. Note the changes in the radial wave numbers in the radial and latitudinal velocity components upon the transition between the prograde and retrograde flows.

The spatial distributions of codensity in both cross-sections suggest an approximate spherical symmetry (rather than cylindrical symmetry or, equivalently, axisymmetry), with the hotter (more buoyant) regions near the inner-core boundary and colder (less buoyant) regions near the core-mantle boundary. The codensity structure does not appear to differ between the retrograde and prograde flow regimes. While the change from retrograde to prograde zonal flows is not seen in the total codensity field, this transition is displayed in an anomaly codensity field obtained by removing the dominant spherically-symmetric component (the component with the spherical harmonic degree $l = 1$ and order $m = 0$) from the codensity field (not shown). The absence of variations of the instantaneous codensity over small scales is most likely due to the relatively strong fluid motions developed in both regimes, allowing the codensity anomalies to mix and favouring the near-spherical symmetry.

The evolution of the total kinetic-energy density, $E_k = \frac{1}{2}\langle \boldsymbol{u}^2 \rangle$, where $\langle \cdot \rangle$ indicates averaging over the spherical shell, is shown in figure 3. The poloidal and toroidal parts of E_k are also indicated, with a notable difference between the retrograde ($Pr = 10^{-3}$) and prograde ($Pr = 10^{-2}$) regimes. Examples of time series shown in figure 3 exhibit oscillations in the

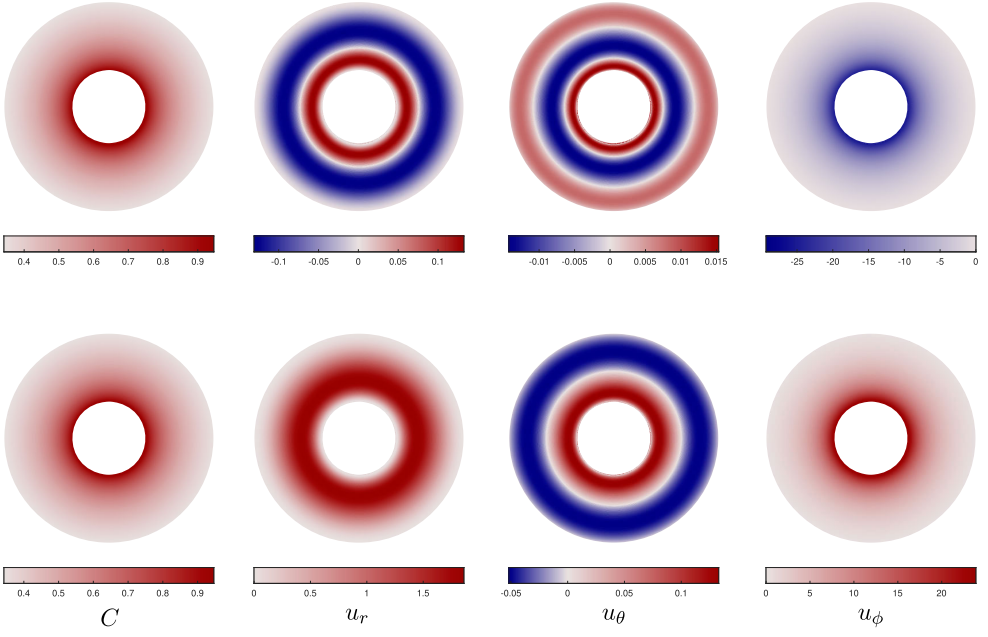

Figure 2. Equatorial cross-sections of the codensity C and the velocity components u_r, u_θ and u_ϕ for $Pr = 10^{-3}$ (top panel; retrograde zonal flow) and $Pr = 10^{-2}$ (bottom panel; prograde zonal flow). The other parameter values are the same as in figure 1.

structure of the azimuthally-averaged toroidal field, while the mean poloidal field shows only a little variation in the amplitude and does not participate in the oscillations. In both regimes, the toroidal component of the velocity dominates the poloidal one. These results are found to be only weakly dependent on Ra/Ra_c. The power spectrum of the velocity field is shown in figure 4, indicating the dominance of the spherically-symmetric component. The contribution of higher harmonics to the resulting flows is found to be larger in the prograde than retrograde regime. To demonstrate the robust nature of a mechanism behind the toroidal velocity oscillations would require more detailed computational results for a wider range of parameters.

One aim of this study is to delineate the conditions for the occurrence of prograde and retrograde fluid flows in the parameter space $(Pr, Ra/Ra_c)$. A total of 35 runs were performed in the region where prograde to retrograde zonal propagation is expected to occur. The results of our search are shown in figure 5, which shows the inferred transition

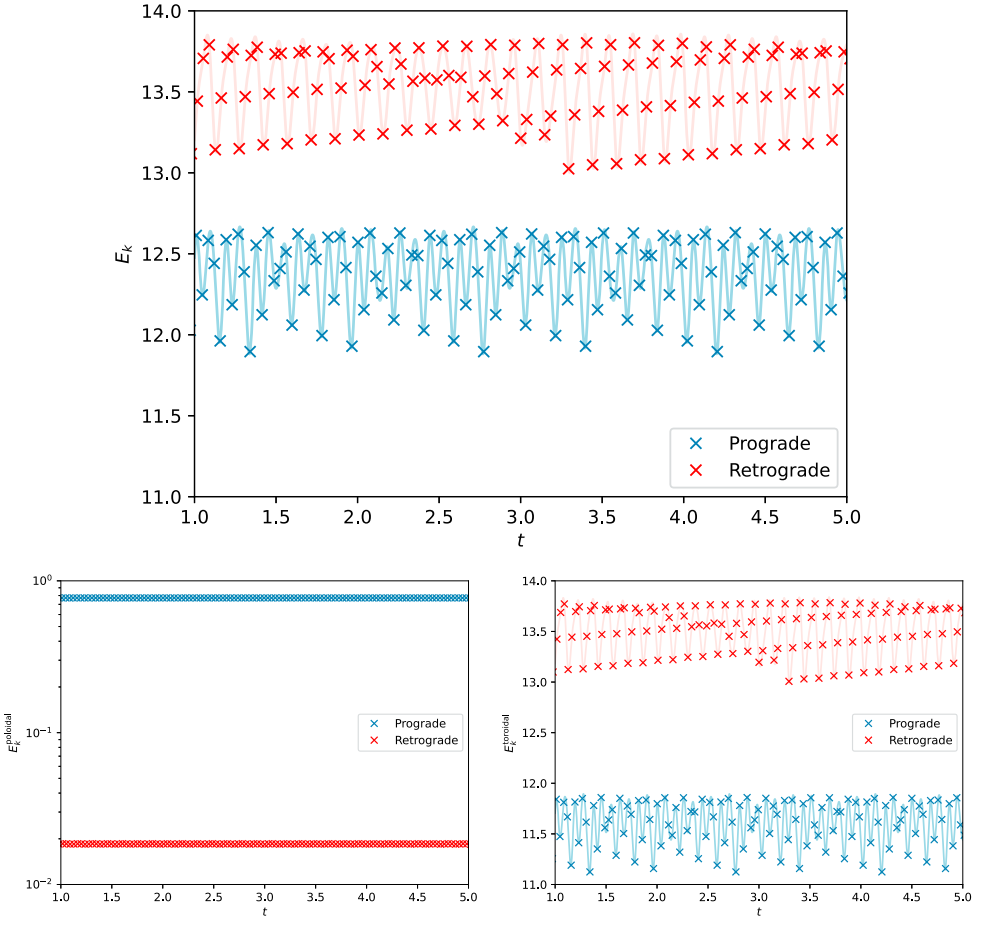

Figure 3. The evolution of the kinetic energy for $Pr = 10^{-3}$ (retrograde zonal flow) and $Pr = 10^{-2}$ (prograde zonal flow). Top panel: the total kinetic energy; bottom panel: the poloidal (left) and toroidal (right) parts of the kinetic energy. The other parameter values are the same as in figure 1.

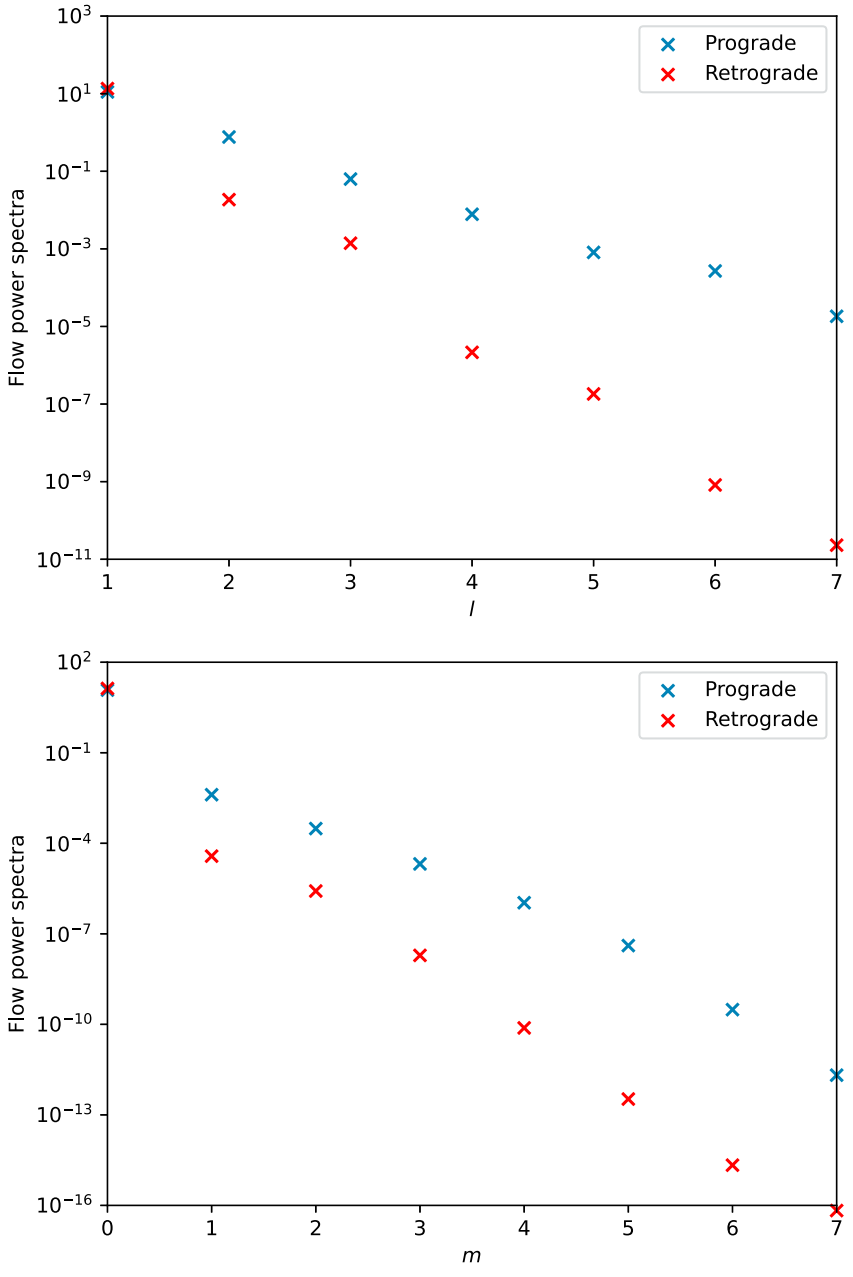

Figure 4. Power spectra of the velocity field as functions of spherical harmonic degree l (top) and order m (bottom) for $Pr = 10^{-3}$ (retrograde zonal flow) and $Pr = 10^{-2}$ (prograde zonal flow). For each l, the sum over all values of m is shown (top). Similarly, for each m, the sum over all values of l is shown (bottom). The other parameter values are the same as in figure 1.

boundary between the prograde and retrograde flows. Unlike Zhang and Busse (1987), Ardes *et al.* (1997), and Horn and Schmid (2017), the prograde propagating wall-attached flows and columnar flows are not observed.

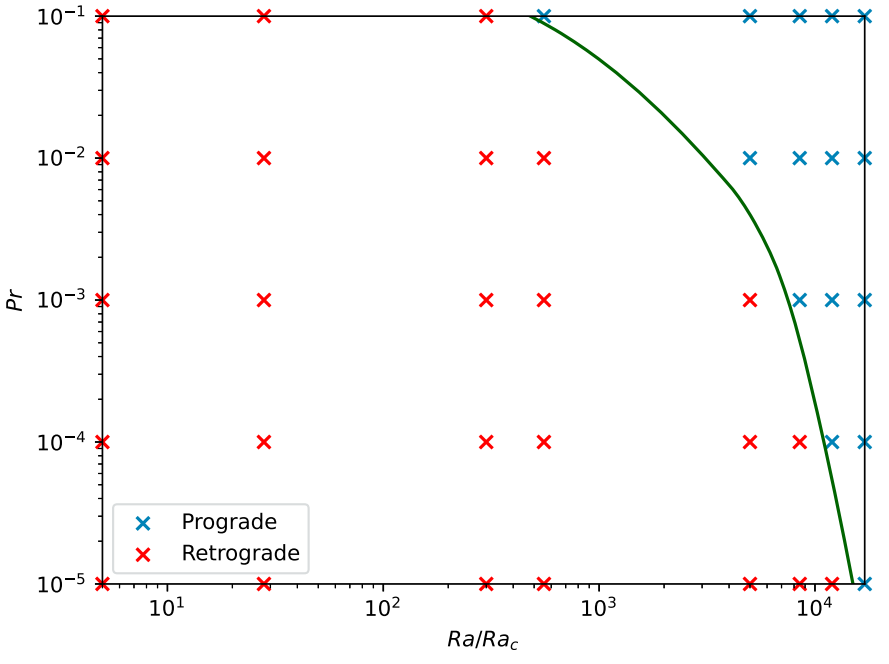

Figure 5. Regime diagram in the parametric space (Ra/Ra_c, Pr). The crosses indicate the points where the numerical simulations were conducted. The inferred curve indicates the points at which a transition between the retrograde and prograde zonal flows occurs. The other parameter values are the same as in figure 1.

4. Conclusions

The inertial, wall-attached and columnar convection structures play an important role in the dynamics of rotating convection irrespective of the buoyancy source (Zhang and Busse 1987, Ardes *et al.* 1997, Horn and Schmid 2017, Pizzi *et al.* 2021). In the fast-rotation, or small- Ekman-number, regime, the wall-attached and columnar convection modes were observed to have a prograde direction of propagation. As the Ekman number decreased, the type of convection changed from inertial to wall-attached and then to columnar; see Zhang and Busse (1987), Ardes *et al.* (1997), Kimura *et al.* (2011), Horn and Schmid (2017), and Šimkanin *et al.* (2018) for further details.

In this contribution, we have studied thermochemical convection in a rotating spherical shell. In the slow-rotation regime considered, we have found that, somewhat surprisingly, not only retrograde but also prograde zonal flows can develop. We have shown that both prograde and retrograde flows have axisymmetric structure dominated by the first harmonic degree, the observation similar to that by Geiger and Busse (1981) in their study of thermal convection in thick spherical fluid shells.

We have mapped out parameter space to identify a transition between the retrograde and prograde zonal propagation of convection structures. The indicator of the change in propagation direction has been a decrease in the kinetic-energy density as the Prandtl number increased, accompanied by an increased contribution of higher harmonics to the momentum balance. We note that the transition in the propagation direction may be

induced also by other mechanisms, including an increase of the inertial effects in the flow (Horn and Schmid 2017). A small difference in the Rossby number between the retrograde and the prograde flows indicates that such a mechanism can be ruled out here.

Disclosure statement

No potential conflict of interest was reported by the author(s).

Funding

This study was supported by the VEGA grant 1/0245/24, the Mobility Project SAV-23-06/CAS-SAS-2022-01 and the Comenius University Grant UK/1170/2024. Computing resources (the SGI cluster NEMO) supporting this work were provided by the institute of Geophysics at the Czech Academy of Sciences.

ORCID

M. Y. Nnaedu http://orcid.org/0000-0002-3133-1895

References

Ardes, M., Busse, F.H. and Wicht, J., Thermal convection in rotating spherical shells. *Phys. Earth Planet. Inter.* 1997, **99**, 55–67.

Aubert, J., Aurnou, J. and Wicht, J., The magnetic structure of convection-driven numerical dynamos. *Geophys. J. Int.* 2008, **172**, 945–956.

Aubert, J., Labrosse, S. and Poitou, C., Modelling the palaeo-evolution of the geodynamo. *Geophys. J. Int.* 2009, **179**, 1414–1428.

Braginsky, S.I. and Roberts, P.H., Equations governing convection in the Earth's core and the geodynamo. *Geophys. Astrophys. Fluid Dynam.* 1995, **79**, 1–97.

Christensen, U.R. and Wicht, J., Models of magnetic field generation in partly stable planetary cores: applications to Mercury and Saturn. *Icarus* 2008, **196**, 16–34.

Christensen, U.R., Aubert, J., Cardin, P., Dormy, E., Gibbons, S., Glatzmaier, G., Grote, E., Honkura, Y., Jones, C., Kono, M., Matsushima, M., Sakuraba, A., Takahashi, F., Tilgner, A., Wicht, J. and Zhang, K., A numerical dynamo benchmark. *Phys. Earth Planet. Inter.* 2001, **128**, 25–34.

Davies, C.J. and Gubbins, D., A buoyancy profile for the Earth's core. *Geophys. J. Int.* 2011, **187**, 549–563.

Dormy, E., Modélisation numérique de la dynamo terrestre. Ph.D. Thesis, Institut de Physique du Globe de Paris, 1997.

Dormy, E., Cardin, P. and Jault, D., MHD flow in a slightly differentially rotating spherical shell, with conducting inner core, in a dipolar magnetic field. *Earth Planet. Sci. Lett.* 1998, **160**, 15–30.

Geiger, G. and Busse, F.H., On the onset of thermal convection in slowly rotating fluid shells. *Geophys. Astrophys. Fluid Dyn.* 1981, **18**, 147–156.

Glatzmaier, G.A. and Roberts, P.H., Simulating the geodynamo. *Contemp. Physics* 1997, **38**, 269–288.

Horn, S. and Schmid, P.J., Prograde, retrograde, and oscillatory modes in rotating Rayleigh-Bénard convection. *J. Fluid Mech.* 2017, **831**, 182–211.

Jones, C.A., Planetary magnetic fields and fluid dynamos. *Annu. Rev. Fluid Mech.* 2011, **43**, 583–614.

Kimura, K., Takehiro, S. and Yamada, M., Stability and bifurcation diagram of Boussinesq thermal convection in a moderately rotating spherical shell. *Phys. Fluids* 2011, **23**, 074101.

Kutzner, C. and Christensen, U.R., From stable dipolar towards reversing numerical dynamos. *Phys. Earth Planet. Int.* 2002, **131**, 29–45.

Lister, J.R. and Buffett, B.A., The strength and efficiency of thermal and compositional convection in the geodynamo. *Phys. Earth Planet. Int.* 1995, **91**, 17–30.

Pizzi, F., Giesecke, A., Šimkanin, J. and Stefani, F., Prograde and retrograde precession of a fluid-filled cylinder. *New. J. Phys.* 2021, **23**, 123016.

Raynaud, R. and Dormy, E., Intermittency in spherical Couette dynamos. *Phys. Rev. E* 2013, **87**, 033011.

Šimkanin, J. and Hejda, P., Magnetic fields generated by hydromagnetic dynamos at the low Prandtl number in dependence on the Ekman and magnetic Prandtl numbers. *Phys. Earth Planet. Int.* 2013, **217**, 22–30.

Šimkanin, J., Kyselica, J. and Guba, P., Inertial effects on thermochemically driven convection in a spherical shell. *Geophys. J. Int.* 2018, **212**, 2194–2205.

Zhang, K., Spiralling columnar convection in rapidly rotating spherical fluid shells. *J. Fluid Mech.* 1992, **236**, 535–556.

Zhang, K.K. and Busse, F.H., On the onset of convection in rotating spherical shells. *Geophys. Astrophys. Fluid Dyn.* 1987, **39**, 119–147.